



Cite this: *J. Mater. Chem. C*, 2018, 6, 11248

Received 28th August 2018,
Accepted 26th September 2018

DOI: 10.1039/c8tc04298e

rsc.li/materials-c

A pure red luminescent β -carboline-substituted biphenylmethyl radical: photophysics, stability and OLEDs†

Alim Abdurahman,[†] Yingxin Chen, Xin Ai,[†] Obolda Ablikim, Yu Gao, Shengzhi Dong, Bao Li,[†] Bing Yang,[†] Ming Zhang and Feng Li^{†*}

Luminescent radicals, whose emission comes from the doublet exited state, have potential application in the field of organic optoelectronics. However, few radicals show luminescence at room temperature. Herein, a new pure red-emissive biphenyl-type (*N*-pyrido[3,4-*b*]indolyl)bis(2,4,6-trichlorophenyl)methyl radical (PyID-BTM) is designed and synthesized, in which the carbazole moiety of CzBTM (a previously reported biphenylmethyl radical by our group) is successfully replaced by β -carboline. Its photophysical properties, including the ground and excited states, and the radiative and non-radiative processes are systematically investigated. The photoluminescence quantum efficiency ($\phi = 19.5\%$) of PyID-BTM is ten times higher than that of CzBTM ($\phi = 2.0\%$) in cyclohexane. The crystal structure, magnetic properties, photostability and electroluminescence performance of PyID-BTM are studied. An optimized OLED device using PyID-BTM as an emissive dopant showed pure red emission with CIE coordinates of (0.649, 0.317) and a maximum EQE of 2.8%, and the formation ratio of doublet excitons was up to 70%. This study provides a new approach for designing high-performance luminescence biphenylmethyl radicals for applications in organic electroluminescence.

Introduction

Owing to their unique chemical and physical properties, open-shell organic radicals have been extensively studied for versatile applications in organic spintronics,^{1–4} organic magnetism,^{5–7} energy storage,⁸ non-linear optics,⁹ catalysts¹⁰ and biological imaging agents.¹¹ Recently, luminescent radicals have attracted more attention due to their emission from the spin-allowed

doublet excited state (D_1),¹² a $D_1 \rightarrow D_0$ transition. Hence, the harvesting of triplet excitons is circumvented in radical-based OLEDs.¹³

To date, there are few radicals that show luminescence at room temperature. Typical examples of these are the triphenylmethyl radicals, such as the perchloro triphenylmethyl (PTM)-cored radicals obtained by Lambert and co-workers,^{14,15} the tris(2,4,6-trichlorophenyl)methyl (TTM) series radicals reported by Juliá *et al.*,^{16,17} and the pyridyl-containing triphenylmethyl radicals (PyBTM) synthesized by Nishihara and co-workers.^{18,19}

It is an important and challenging task to develop a new stable room-temperature luminescent radical system for extending the application of radicals in organic optoelectronics. To our delight, we have recently reported a novel stable room-temperature luminescent biphenylmethyl radical, (*N*-carbazolyl)bis(2,4,6-trichlorophenyl)-methyl radical (CzBTM),²⁰ which has provided a new path for luminous radical systems. However, although CzBTM has high thermal and photostability, the fluorescence quantum yield in cyclohexane is only 2.0%. Through calculations, we found that the non-radiative decay of CzBTM is relatively large, which is probably due to the strong vibronic coupling between the carbazole and the central radical. Since carbazole is a medium electron-donating group, what would happen if the weak electron-donating group attached to bis(2,4,6-trichlorobenzyl)methyl instead of carbazole? Can this change reduce the vibronic coupling of molecules and thus improve the photophysical properties of the biphenylmethyl radicals? As the reaction mechanism for the synthesis of biphenylmethyl radicals is rather special, many of the donor moieties we tried could not react with 2,2'-(bromomethylene)bis(1,3,5-trichlorobenzene) (HBTM-Br) by this reaction mechanism. We found that the success of this reaction is closely related to the activity of the hydrogen at the nitrogen in the substituent group.

The β -carboline moiety is composed of a conjugated pyridine and indole unit and has better electron transporting properties than carbazole due to the electron deficiency of the pyridine unit. The good electron deficiency of β -carboline could balance the holes and electrons, and could improve the quantum efficiency of

State Key Laboratory of Supramolecular Structure and Materials, College of Chemistry, Institute of Theoretical Chemistry, Jilin University, Qianjin Avenue 2699, Changchun, 130012, P. R. China. E-mail: lifeng01@jlu.edu.cn
† Electronic supplementary information (ESI) available. CCDC 1831917. For ESI and crystallographic data in CIF or other electronic format see DOI: 10.1039/c8tc04298e

OLEDs.²¹ In this work, we successfully reacted β -carboline with HBTM-Br and obtained a pure red-emissive biphenyl-type radical (N-pyrido[3,4-*b*]indolyl)bis(2,4,6-trichlorophenyl)methyl (PyID-BTM). To our knowledge, PyID-BTM is the first example of a biphenyl-methyl radical that successfully links a weak electron-donating group, and the second reported biphenylmethyl-type radical. Comparative photophysical studies on PyID-BTM and CzBTM reveal that PyID-BTM shows a ten times higher photoluminescence quantum efficiency ($\phi = 19.5\%$) than that of CzBTM ($\phi = 2.0\%$) in cyclohexane. We also studied the magnetic properties and photostability of PyID-BTM. It is worth noting that the OLED based on PyID-BTM (used as an emissive dopant) exhibits a pure red color index of (0.667,0.330) and a maximum EQE of 2.8%.

Results and discussion

Synthesis and characterization

Scheme 1 shows the synthesis route of the intermediates and target radical PyID-BTM. The synthetic details of the compounds are provided in the ESI†. 1,2,3,4-tetrahydro- β -carboline (M1) was obtained by the Pictet-Spengler cyclization of tryptamine with formaldehyde. Then (M1) was oxidized to β -carboline (PyID) by refluxing with Pd-C in xylenes. HBTM-Br was attained by a two step reaction with high yield according to our previous report.²⁰ Then, PyID-BTM was synthesized *via* the same reaction mechanism with CzBTM and was characterized by MALDI-TOF mass spectrometry, elemental analysis, and Fourier transform infrared spectroscopy (FTIR) (see the ESI†). The molecular structure of the radical was determined by single crystal X-ray diffraction (Fig. 1a and Table S1, ESI†). The existence of spin $S = 1/2$ was confirmed by electron paramagnetic resonance (EPR) spectroscopy at room temperature (Fig. 1b). In addition, magnetic susceptibility measurements for PyID-BTM powder were carried out with a superconducting quantum interference device (SQUID) magnetometer over the range 2–300 K using a 1000 Oe field strength. Fig. 2 shows the plot of the χ_m - T curve of PyID-BTM. The susceptibility reasonably follows the Curie-Weiss law, with the best fit giving a Weiss constant $\theta = -4.8$ K, and a Curie constant $C = 0.385$ emu mol⁻¹. These results indicate that the radical PyID-BTM is paramagnetic with

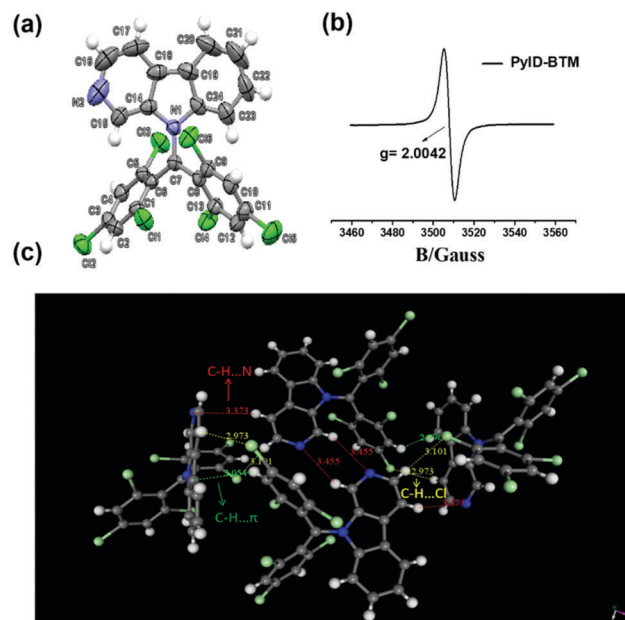


Fig. 1 (a) Molecular structure of crystalline PyID-BTM with thermal ellipsoids set at 50% probability. (b) EPR spectrum of PyID-BTM in cyclohexane solution at 298 K. (c) The weak interactions in the crystal.

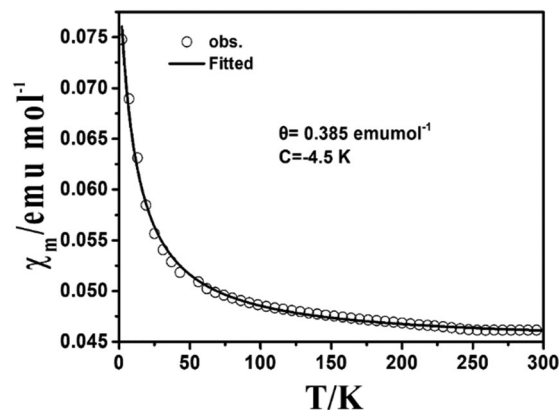
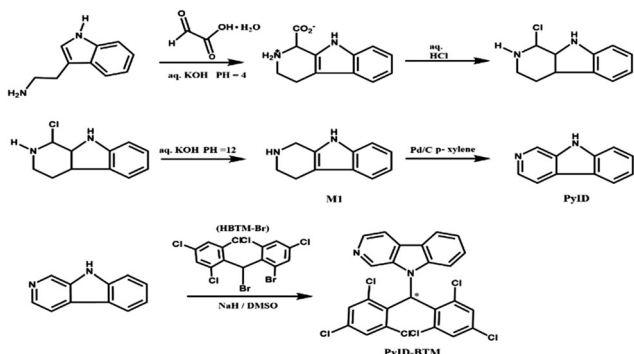


Fig. 2 Observed (circle) and fitted (line) χ_m - T curve of PyID-BTM.

weak spin-spin interactions. The measured value of the Curie constant $C = 0.385$ is in good agreement with the expected value of 0.375 emu mol⁻¹ for a $S = 1/2$ organic radical.

X-ray crystallographic analysis

A single crystal of PyID-BTM was obtained by slow evaporation from the chloroform/ethanol solution at room temperature. Single crystal X-ray diffraction shows that the central methyl carbon atoms are sp² hybridized and are shielded sterically by four halogen atoms (Fig. 1a), and C7 and its three neighboring atoms N1, C6 and C8 lie in the same plane. The three aromatic rings are held in a propeller-like conformation due to steric hindrance from the chlorine atoms. The bond angles and dihedral angles are similar to those of CzBTM (Table S2, ESI†). The crystal is constructed by multiple CH... π , CH...N and CH...Cl interactions, which are summarized in Fig. 1c.



Scheme 1 Synthesis route of the biphenylmethyl radical PyID-BTM.

Thermal and electrochemical properties

The thermal properties of PyID-BTM were investigated with thermogravimetric analysis (TGA) under a nitrogen atmosphere (see Fig. S3 in the ESI†). The decomposition temperature (T_d corresponding to 5% weight loss) for PyID-BTM is 241 °C, which is higher than that of CzBTM (230 °C). The good thermal stability of PyID-BTM could be caused by the rigid molecular structure and strong intermolecular interaction imparted by nitrogen atoms at the pyridine unit.

The energy levels of the frontier orbitals (α -SOMOs and β -SUMOs) of PyID-BTM were examined by cyclic voltammetry (CV) in CH_2Cl_2 with 0.1 M TBAPF₆ as a supporting electrolyte. The results of the CV measurements are shown in Fig. S4 (ESI†). The energy level of the α -SOMO of PyID-BTM is obtained to be -4.83 eV from the oxidation potential, which is lower than the α -SOMO level of CzBTM (-4.71 eV). From the reduction potential of the CV curves, the β -SUMO levels of PyID-BTM and CzBTM were obtained to be -3.76 eV and -3.71 eV, respectively. These data indicate that the replacement of β -carboline leads to a lowering of the frontier energy levels of the radical PyID-BTM. These results were further confirmed by DFT calculations which are shown in the next section. We also performed 20 cycles of a CV scan on PyID-BTM and there were no changes found in the redox peaks (also see Fig. S5 in the ESI†).

Density functional theory simulation

Frontier molecular orbitals (MOs) were calculated using DFT methods (UB3LYP/6-31G(d,p)). The spin density distributions of PyID-BTM are similar to those of CzBTM (see Fig. S6 in the ESI†). The calculated MO results show (Fig. 3) that the α -SOMO and β -SUMO (136α and 136β) of PyID-BTM and CzBTM are mainly delocalized on the central carbon atom and extended to the aromatic rings. The energy level of the α -SOMO of PyID-BTM (-5.15 eV) is lower than that of CzBTM (-4.99 eV) and the β -SUMO of PyID-BTM (-3.13 eV) is also lower than that of CzBTM (-3.01 eV). In PyID-BTM, the α and β -lowest unoccupied molecular orbitals (LUMO; 137α and 137β) are mainly delocalized over the two benzene rings which are similar to those of CzBTM. However, the α and β -highest occupied molecular orbitals (HOMO; 135α and 135β) are delocalized over the two benzene rings and

carboline moieties, which is different from CzBTM where the HOMOs are mainly delocalized over the carbazole moiety. The DFT results of the decreasing energy levels after the replacement of β -carboline are in agreement with the electrochemical results. We expect that these could improve the photophysical properties of the radical.

Photophysical properties

Fig. 4a shows the UV/vis absorption and emission spectra of PyID-BTM in cyclohexane. For comparison, the photophysical properties of CzBTM were also measured. The summarized photophysical data of PyID-BTM and CzBTM are listed in Table 1. PyID-BTM exhibits three main absorption bands: a strong absorption band at 260 nm, caused by β -carboline, which has a 30 times higher molar extinction coefficient (ϵ) than that of the band at 284 nm caused by carbazole in CzBTM, and also has a blue shift of 24 nm; a medium absorption band at 383 nm which has a blue shift of 4 nm and has a 2.3 times higher ϵ compared with that of CzBTM; a weak and broad absorption band with two peaks at 510 nm and 550 nm, which are blue-shifted by 4 nm compared to the two peaks of CzBTM at 514 nm and 554 nm, and their ϵ values are also 2.3 and 2.1 times higher, respectively. Time-dependent DFT calculation (TD-DFT) results shows that the medium (383 nm) and weak (510 and 554 nm) absorption bands could be attributed to the transition from 133β to 136β , 134β to 136β and 135β to 136β , respectively. PyID-BTM in cyclohexane displayed one emission band (664 nm) upon excitation at 550 nm, which is blue-shifted by 33 nm compared with that of CzBTM (697 nm). The absolute photoluminescence quantum yield (ϕ) of PyID-BTM in cyclohexane solution is 19.5%, which is ten times higher than that of CzBTM ($\phi = 2.0\%$). We also performed transient PL decay measurements of PyID-BTM in cyclohexane solution (Fig. 4b). The measurement results revealed that PyID-BTM showed a single exponential decay with a lifetime (τ) of 12.8 ns, which was three times longer than that of CzBTM (4.0 ns), which led to an improved photoluminescence quantum yield.¹⁹ According to the results of ϕ and τ , the radiative rate constants (k_r) and non-radiative rate constants (k_{nr}) of PyID-BTM and CzBTM were calculated using basic photophysical equations (1) and (2) (Table 1).

$$\phi = k_r / (k_r + k_{nr}) \quad (1)$$

$$\tau = 1 / (k_r + k_{nr}) \quad (2)$$

The calculation results show that the k_r and k_{nr} values of PyID-BTM are three times higher than and one quarter of those of CzBTM, respectively. These two factors can explain why PyID-BTM exhibits a good photoluminescence efficiency. The increase of k_r of PyID-BTM is due to the higher molar extinction coefficient (oscillator strength) at the excited transition (Fig. 4a, Table 1 and Fig. S7, S8 in the ESI†). The TD-DFT calculation results also proved that there is a higher oscillator strength in PyID-BTM.

The decrease of k_{nr} of PyID-BTM can be explained by energy gap law. Replacing the carbazole moiety with an electron-withdrawing

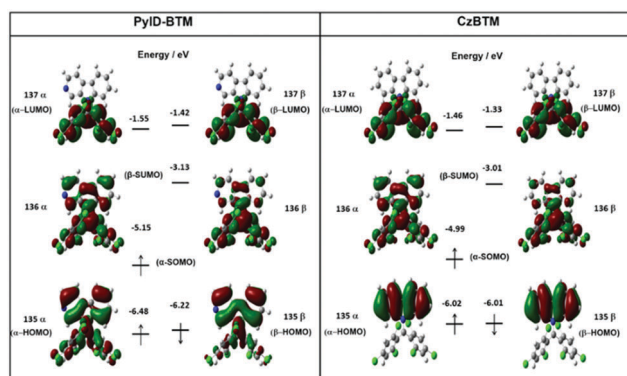


Fig. 3 Frontier orbitals of PyID-BTM and CzBTM using DFT methods (UB3LYP/6-31G(d,p)).

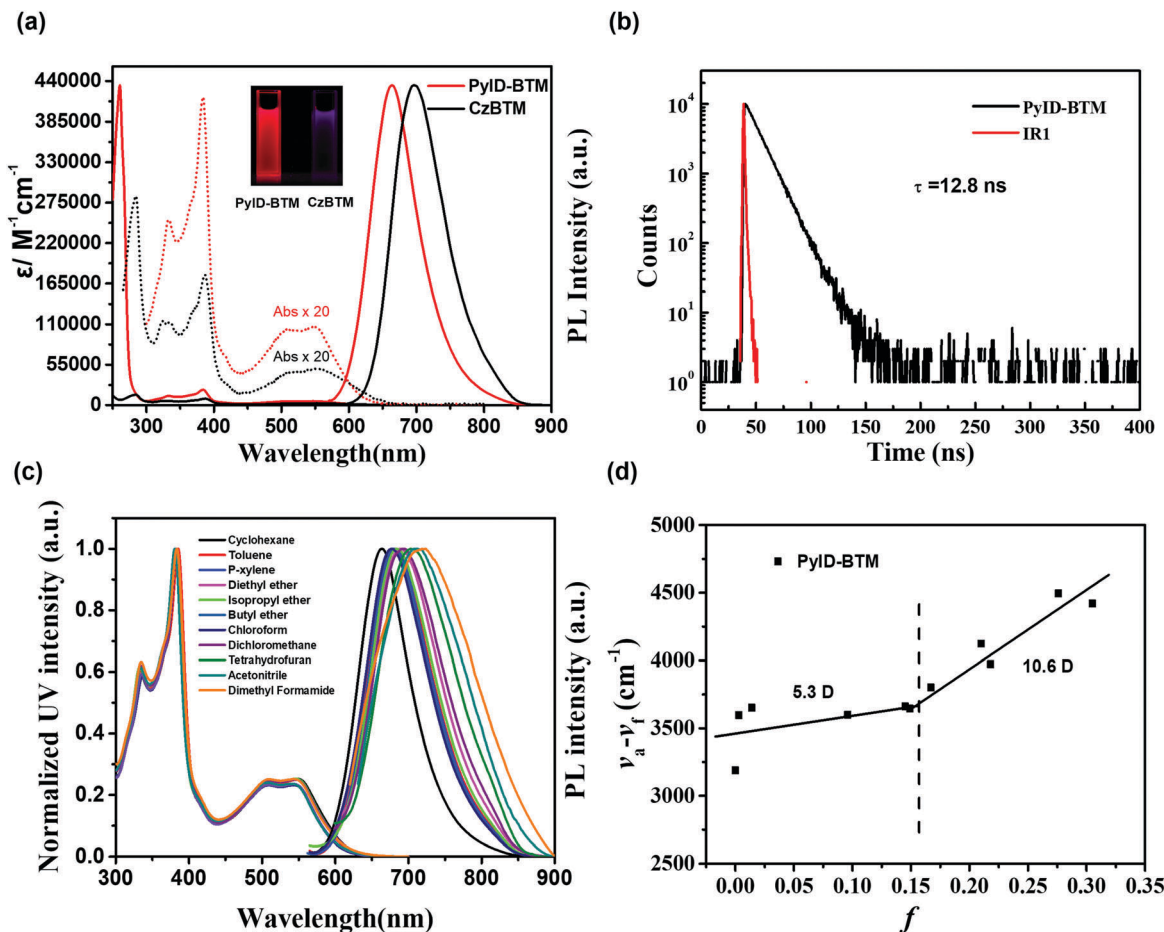


Fig. 4 (a) Absorption and emission spectra of PyID-BTM and CzBTM in cyclohexane solution (10^{-6} M) (the inset shows the photographs of PyID-BTM (left) and CzBTM (right) in cyclohexane solution (10^{-5}) under irradiation (365 nm) with a UV lamp at room temperature). (b) PL decay of PyID-BTM in cyclohexane under ambient conditions. (c) Normalized absorption and emission spectra of PyID-BTM in various solvents (10^{-5} M) at room temperature. (d) Linear correlation of the orientation polarization (Δf) of solvent media with the Stokes shift ($\nu_a - \nu_f$), where a: absorbed light and f: fluorescence, for PyID-BTM (see Table S3 (ESI[†]) for the solvents and corresponding data).

Table 1 Photophysical parameters of PyID-BTM and CzBTM in cyclohexane

Molecule	$\lambda_{\text{abs}}^a/\text{nm}$ ($\epsilon/\text{M}^{-1} \text{cm}^{-1}$)	λ_{PL}^a (nm)	Φ_f^b	τ^c (ns)	k_r ($\times 10^6 \text{s}^{-1}$)	k_{nr} ($\times 10^6 \text{s}^{-1}$)
CzBTM	284(1.42×10^4)/387(8.99×10^3) 514(2.24×10^3)/554(2.47×10^3)	697	0.020	4.0	5.0	245
PyID-BTM	260(4.36×10^5)/383(2.11×10^4) 510(5.17×10^3)/550(5.29×10^3)	664	0.195	12.8	13.9	64

^a Measured in cyclohexane at room temperature. ^b Relative PLQYs were measured using an integrating spectrophotometer. ^c The lifetimes in cyclohexane were measured using an Edinburgh fluorescence spectrometer (FLS980) under laser excitation at 378.8 nm and a pulse width of 68.9 ps.

unit such as β -carboline leads to an increase in the D_0 - D_1 energy gap of PyID-BTM, which was confirmed by the DFT calculations and the absorption and emission spectra. The large energy gap of PyID-BTM could reduce the Frank-Condon factors, which indicates a decrease in internal conversion and, as a result, k_{nr} decreases. In order to further support this conclusion, the internal conversion of the radicals was calculated by the MOMAP (Molecular Materials Property Prediction Package) program.^{23,24} The calculation results showed that the internal conversion of PyID-BTM ($2.60 \times 10^{11} \text{s}^{-1}$) was two times slower than that of CzBTM ($5.16 \times 10^{11} \text{s}^{-1}$).

To investigate the frontier orbital (D_0 and D_1 state) properties of PyID-BTM, UV-vis absorption and photoluminescence (PL) were measured in various solvents with different polarities. As displayed in Fig. 4c and Table S3 (ESI[†]), UV-vis absorption did not change much upon increasing the solvent polarity, thus indicating a rather small dipolar change at the ground state in different polar solvents. However, the PL spectra displays an obviously bathochromic shift and the emission intensity decreases as the solvent polarity increases. To further understand the effect of solvent polarity on the excited state of

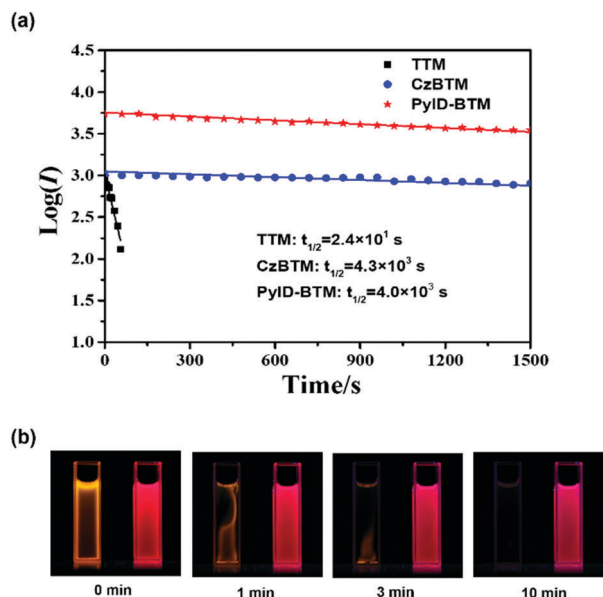


Fig. 5 (a) Comparison of the fluorescence decay of TTM, CzBTM and PyID-BTM in cyclohexane under irradiation with a 355 nm pulse laser (power density: 366.4 kW cm^{-2} , pulse width: 8 ns, frequency: 10 Hz). (b) Photographs of TTM (left cuvette in each image) and PyID-BTM (right cuvette) in cyclohexane solution ($5 \times 10^{-5} \text{ M}$) under irradiation (365 nm) with a UV lamp at room temperature under ambient conditions.

PyID-BTM, we used the Lippert–Mataga model. Fig. 4d shows the plot of the orientation polarizability (Δf) versus the Stokes shift ($\nu_a - \nu_f$). The linear fitting results showed that PyID-BTM displays two sections of linear relationship for the low-polarity solvents ($f < 0.15$) and high-polarity solvents ($f > 0.15$). The dipole moments were calculated to be 5.3 D and 10.6 D for the low and high Δf regions, respectively. As the small dipole moment and higher photoluminescence quantum yield appear in the low Δf regions, we believed that the emission of PyID-BTM mainly comes from the locally excited (LE) state in the low-polarity solvents. The large dipole moment and low photoluminescence quantum yield of PyID-BTM in the high Δf regions indicates that a charge transfer (CT) state is dominant in the high-polarity solvents.

Photostability of radicals

Photostability, one of the important properties of luminescent radicals, was measured by recording the decay of the fluorescence intensity in cyclohexane solution with the irradiation of a pulse laser at 355 nm with a power density of 366.4 kW cm^{-2} . The results show that (Fig. 5a) PyID-BTM displays excellent photostability, which is similar to that of CzBTM, and is 160 times more stable than TTM. To the best of our knowledge, the estimated half-life ($t_{1/2}$) of PyID-BTM is the most outstanding value to date for luminescent radicals with a fluorescence quantum yield up to 20%.^{25,26}

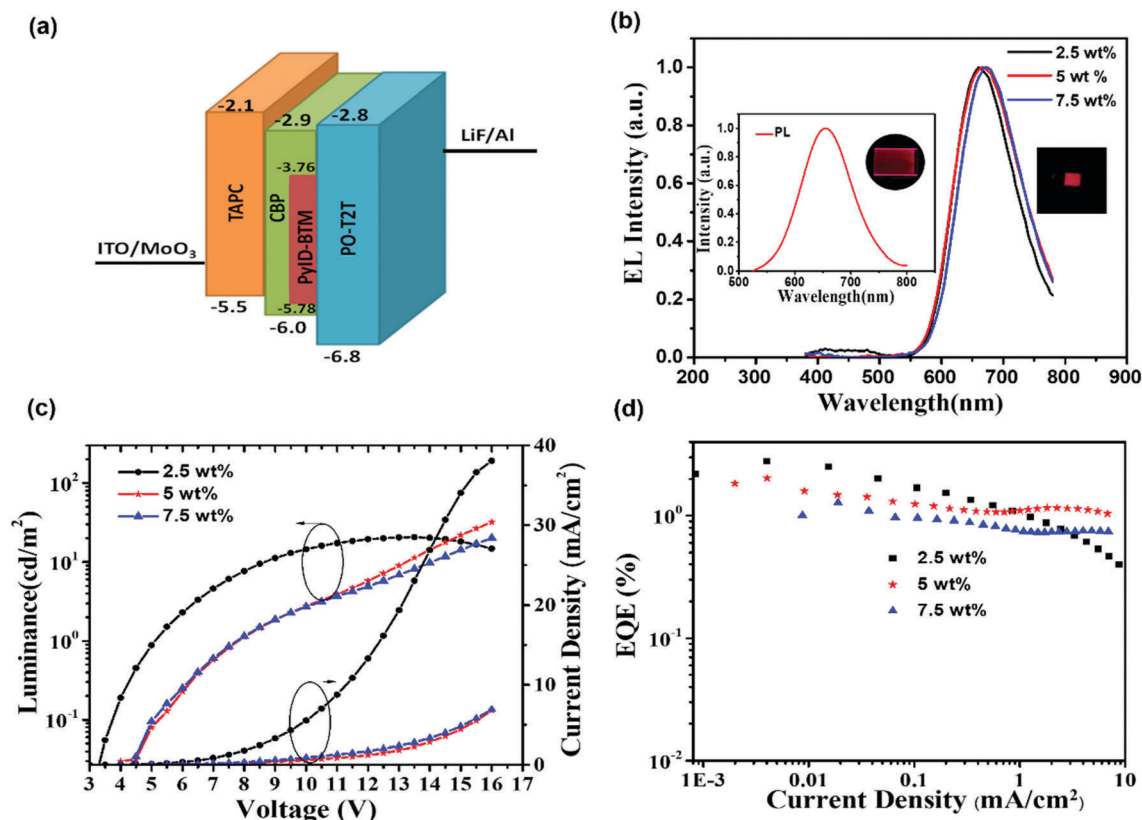


Fig. 6 (a) The energy-level diagram and the schematic representation of the OLED architecture. (b) The EL spectra (5 V) of the devices with three different doping concentrations of PyID-BTM in CBP (the inset shows the photograph of the (CBP:PyID-BTM 5 wt%) device operating at 7 V and the PL spectra of the PyID-BTM 5 wt% doped film in CBP excited at 333 nm). (c) Current density–voltage–luminance (J – V – L) characteristics of the devices. (d) External quantum efficiency versus current density.

Table 2 Electroluminescence performance of the devices

Device	wt ^a (%)	Φ_{PL}^b (%)	V_{on}^c [V]	EQE ^d (%)	λ_{EL}^e	CE ^f (cd A ⁻¹)	L_{max} (cd m ⁻²)	PE ^g (lm W ⁻¹)	CIE(x, y)
I	2.5	13.7	3.5	2.8	660	1.4	21.2	1.2	(0.649, 0.317)
II	5	9.4	4.0	2.0	666	0.9	31.8	0.6	(0.667, 0.330)
III	7.5	7.3	4.5	1.3	672	0.5	22.5	0.3	(0.671, 0.326)

^a Doping concentration of PyID-BTM in CBP. ^b PL quantum yield of the thin film (50 nm) measured using an integrating spectrophotometer. ^c Turn-on voltage. ^d The maximum external quantum efficiency. ^e The maximum EL wavelength. ^f Maximum current efficiency. ^g Maximum power efficiency.

Electroluminescence properties

To evaluate the potential application of PyID-BTM for light emission, OLEDs with the following architecture were fabricated: indium tin oxide (ITO)/MoO₃ (3 nm)/4,4'-cyclohexylidenebis[*N,N*-bis-(*p*-tolyl)aniline] (TAPC) (70 nm)/4,4'-bis(*N*-carbazolyl)-1,1'-biphenyl (CBP):PyID-BTM (*x* wt%, 40 nm)/2,4,6-tris[3-(diphenylphosphoryl)phenyl]-1,3,5-triazine (PO-T2T) (70 nm)/LiF (0.8 nm)/Al (100 nm). In these devices, ITO was the anode, Al was the cathode, TAPC played the role of the hole-transporting layer (HTL), and PO-T2T served as an electron-transporting layer (ETL). MoO₃ and LiF were used to improve the charge injection. PyID-BTM doped into CBP was used as the emitting layer (EML), where *x* was equal to 2.5, 5 and 7.5%. The three different concentrations of the devices were defined as device I, device II and device III, respectively. The energy-level diagram and the schematic representation of the OLED architecture are shown in Fig. 6a. Important EL data and the partial performance curves of the devices are presented in Fig. S9 (ESI†) and Table 2.

As can be seen from Fig. 6b, the three devices display pure red emission, and electroluminescence (EL) wavelength peaks at 660 nm, 666 nm, and 672 nm, respectively, demonstrating that a little redshift in the EL spectra occurs when the doping concentration of PyID-BTM is increased in the CBP host. The EL spectra matched well with the PL spectra of the CBP:PyID-BTM (5 wt%) thin film (Fig. 6b), indicating that the EL emission from the device comes from the radiative decay of the doublets of PyID-BTM. The normalized EL spectra of device II and III were almost unchanged as the driving voltage increased from 4.5 V to 16 V for the devices. However, a tiny wide emission band arose in the blue-green region (400–550 nm) (Fig. S10, ESI†), which was relatively obvious in device I. The blue-green emission could come from the exciplex emission between CBP and PO-T2T.^{26,27}

The Commission Internationale de L'Eclairage (CIE) coordinate value of device I is (0.649, 0.317) at 5 V, and those of device II and III are (0.667, 0.330), and (0.671, 0.326) at 7 V, respectively. These are very close to the red standard CIE coordinate (0.670, 0.330) requirements defined by the National Television System Committee (NTSC). The current density–voltage–luminance (*J*–*V*–*L*) characteristics are shown in Fig. 6c. The turn-on voltages of the three doping concentration devices are 3.5 V, 4 V and 4.5 V, respectively. The results showed that the turn-on voltage depends on the doping concentration.

As can be seen from Fig. 6d, the highest EQE value was observed from device I (2.8%). The maximum EQE values for device II and III were 2.0% and 1.3%, respectively. If the out-coupling efficiency is

assumed to be 30%, according to spin statistics, the formation ratios of doublet excitons of the three devices are estimated to be 68%, 72% and 59%, respectively. Fig. S11 (ESI†) shows the EPR spectrum of the PyID-BTM powder before and after evaporation. The EPR results indicate that evaporation does not wreak havoc with the unpaired electrons of PyID-BTM.

Conclusion

We prepared a new biphenylmethyl-type stable luminescent radical PyID-BTM. PyID-BTM exhibited a ten times higher photoluminescence quantum yield than previously reported CzBTM in cyclohexane solution. The preferable luminescence properties of PyID-BTM were attributed to the higher molar extinction coefficient and the slower internal conversion resulting from a β -carboline substituent instead of a carbazole moiety. PyID-BTM exhibited excellent photostability, which was comparable with CzBTM. The doped OLEDs based on PyID-BTM showed pure red emission. It is noteworthy that the device with 2.5% doping concentration of PyID-BTM in the CBP host achieved a maximum EQE of 2.8% and the formation ratio of doublet excitons of the device was up to 70%. Our study provides a new pathway for designing high-performance luminescence biphenylmethyl radicals for organic electroluminescence applications.

Conflicts of interest

There are no conflicts to declare.

Acknowledgements

We are grateful for the financial support from the National Natural Science Foundation of China (Grant No. 51673080), the National Key R&D Program of China (Grant No. 2016YFB0401001) and the National Key Basic Research and Development Program of China (973 program, Grant No. 2015CB655003) funded by MOST.

Notes and references

- 1 A. R. Rocha, V. M. Garcia-Suarez, S. W. Bailey, C. J. Lambert, J. Ferrer and S. Sanvito, *Nat. Mater.*, 2005, **4**, 335.
- 2 Y. W. Son, M. L. Cohen and S. G. Louie, *Phys. Rev. Lett.*, 2006, **97**, 216803.
- 3 M. Mastorrent, N. Crivillers, C. Rovira and J. Veciana, *Chem. Rev.*, 2011, **112**, 2506.

- 4 R. Frisenda, R. Gaudenzi, C. Franco, M. Mastorrent, C. Rovira, J. Veciana, I. Alcon, S. T. Bromley, E. Burzuri and H. V. D. Zant, *Nano Lett.*, 2015, **15**, 3109.
- 5 K. Awaga and Y. Maruyama, *J. Chem. Phys.*, 1989, **91**, 2743.
- 6 A. J. Banister, N. Bricklebank, I. Lavender, J. M. Rawson, C. I. Gregory, B. K. Tanner, W. Clegg, M. R. J. Elsegood and F. Palacio, *Angew. Chem., Int. Ed.*, 1996, **108**, 2648.
- 7 M. Chikamatsu, T. Mikami, J. Chisaka, Y. Yoshida, R. Azumi, K. Yase, A. Shimizu, T. Kubo, Y. Morita and K. Nakasuji, *Appl. Phys. Lett.*, 2007, **91**, 605.
- 8 Y. Morita, S. Nishida, T. Murata, M. Moriguchi, A. Ueda, M. Satoh, K. Arifuku, K. Sato and T. Takui, *Nat. Mater.*, 2011, **10**, 947.
- 9 K. Kamada, K. Ohta, T. Kubo, A. Shimizu, Y. Morita, K. Nakasuji, R. Kishi, S. Ohta, S. Furukawa and H. Takahashi, *Angew. Chem., Int. Ed.*, 2007, **46**, 3544.
- 10 Q. Cao, L. M. Dornan, L. Rogan, N. L. Hughes and M. J. Muldoon, *Chem. Commun.*, 2014, **50**, 4524.
- 11 M. A. Sowers, J. R. McCombs, Y. Wang, J. T. Paletta, S. W. Morton, E. C. Dreaden, M. D. Boska, M. F. Ottaviani, P. T. Hammond and A. Rajca, *Nat. Commun.*, 2015, **5**, 5460.
- 12 J. Han, Y. Jiang, A. Obolda, P. Duan, F. Li and M. Liu, *J. Phys. Chem. Lett.*, 2017, **38**, 5865.
- 13 Q. Peng, A. Obolda, M. Zhang and F. Li, *Angew. Chem., Int. Ed.*, 2015, **54**, 7091.
- 14 A. Heckmann, C. Lambert, M. Goebel and R. Wortmann, *Angew. Chem., Int. Ed.*, 2004, **43**, 5851.
- 15 A. Heckmann and C. Lambert, *J. Am. Chem. Soc.*, 2007, **129**, 5515.
- 16 V. Gamero, D. Velasco, S. Latorre, F. López-Calahorra, E. Brillas and L. Juliá, *Tetrahedron Lett.*, 2006, **47**, 2305.
- 17 D. Velasco, S. Castellanos, M. López, F. López-Calahorra, E. Brillas and L. Juliá, *J. Org. Chem.*, 2007, **72**, 7523.
- 18 Y. Hattori, T. Kusamoto and H. Nishihara, *Angew. Chem., Int. Ed.*, 2014, **53**, 11845.
- 19 Y. Hattori, T. Kusamoto and H. Nishihara, *Angew. Chem., Int. Ed.*, 2015, **54**(12), 3731.
- 20 X. Ai, Y. Chen, Y. Feng and F. Li, *Angew. Chem., Int. Ed.*, 2018, **57**, 2869.
- 21 Y. Im and J. Y. Lee, *Synth. Met.*, 2015, **209**, 24.
- 22 N. J. Turro, *Modern Molecular Photochemistry*, University Science Books, 1991.
- 23 Y. Niu, W. Li, Q. Peng, H. Geng, Y. Yi, L. Wang, G. Nan, D. Wang and Z. Shuai, *Mol. Phys.*, 2018, **116**, 1078.
- 24 D. Fan, Y. Yi, Z. Li, W. Liu, Q. Peng and Z. Shuai, *J. Phys. Chem. A*, 2015, **119**, 5233.
- 25 Y. Gao, A. Obolda, M. Zhang and F. Li, *Dyes Pigm.*, 2017, **139**, 644.
- 26 Y. Gao, W. Xu, H. Ma, A. Obolda, W. Yan, S. Dong, M. Zhang and F. Li, *Chem. Mater.*, 2017, **29**, 6733.
- 27 A. Obolda, X. Ai, M. Zhang and F. Li, *ACS Appl. Mater. Interfaces*, 2016, **8**, 35472.